

miR-10b-5p regulates venous endothelial cells in deep venous thrombosis by targeting MFG-E8

Ping Li^{1,2}, Qingyun Liu^{1,3}, Zhenhua Huang^{1,3}, Yakun Liu^{1,3}, Feifei Tang^{1,3}, Sihai Gao^{1,3}

¹Division of Cardiothoracic and Vascular Surgery, Heart-Lung Transplantation Center, Sino-Swiss Heart-Lung Transplantation Institute, Tongji Hospital, Tongji Medical College of Huazhong University of Science and Technology, Wuhan, Hubei 430030, P.R. China

²Department of Cardiovascular Surgery, Union Hospital, Tongji Medical College of Huazhong University of Science and Technology, Wuhan, Hubei 430022, P.R. China

³Key Laboratory of Organ Transplantation, Ministry of Education, Key Laboratory of Organ Transplantation, Ministry of Health, Tongji Hospital, Tongji Medical College of Huazhong University of Science and Technology, Wuhan, Hubei 430030, P.R. China

Submitted: 18 December 2022; **Accepted:** 26 February 2023

Online publication: 26 March 2023

Arch Med Sci

DOI: <https://doi.org/10.5114/aoms/161674>

Copyright © 2023 Termedia & Banach

Corresponding author:

Sihai Gao

Division of Cardiothoracic and Vascular Surgery
Heart-Lung Transplantation Center

Sino-Swiss Heart-Lung Transplantation Institute
Tongji Hospital

Tongji Medical College of Huazhong University of Science and Technology

Wuhan, Hubei 430030, P.R. China

Phone: 86-13707129205

E-mail: gshai@tjh.tjmu.edu.cn

Abstract

Introduction: Deep vein thrombosis (DVT) is a common venous thromboembolic disease with an unclear pathogenesis. miR-10b-5p expression was increased in DVT patients and this study aims to determine the functional mechanism of miR-10b-5p in DVT development.

Material and methods: Rats were injected with miR-10b-5p and MFG-E8 related plasmids before DVT model establishment. The thrombus length, weight and size were measured. TUNEL staining was used to detect apoptosis of vascular endothelial cells. Cell transfection on human umbilical vein endothelial cells (HUVECs) was performed to achieve miR-10b-5p suppression and/or MFG-E8 suppression. The cell viability, migration, angiogenesis ability and cell apoptosis of HUVECs were measured. The expression levels of miR-10b-5p, MFG-E8, JAK/STAT signal pathway related proteins in peripheral blood of DVT patients, rats, and HUVECs were detected by RT-qPCR and Western blot.

Results: DVT patients showed increased expression of miR-10b-5p and decreased expression of MFG-E8. miR-10b-5p expression was negatively correlated with MFG-E8. Rats with inhibition of miR-10b-5p or overexpression of MFG-E8 had less deteriorated thrombus, decreased thrombus length and weight, cell apoptosis and suppressed ratios of p-JAK/JAK and p-STAT3/STAT3. miR-10b-5p can negatively regulate and target MFG-E8 in HUVECs. HUVECs transfected with miR-10b-5p inhibitor had increased cell viability, migration and angiogenesis ability as well as suppressed cell apoptosis and decreased p-JAK/JAK and p-STAT3/STAT3 ratios, while co-transfection of miR-10b-5p inhibitor and MFG-E8 suppression could partially counteract the miR-10b-5p inhibitor.

Conclusions: Elevated expression of miR-10b-5p and decreased MFG-E8 expression were found in peripheral blood of DVT patients and inhibition of miR-10b-5p or overexpression of MFG-E8 could attenuate DVT in rat models.

Key words: deep vein thrombosis, miR-10b-5p, MFG-E8, HUVEC, JAK/STAT signal pathway.

Introduction

Venous thromboembolism (VTE) refers to occlusive clot development in the veins, and when the clot formation occurs in the leg it is called deep vein thrombosis (DVT) [1, 2]. VTE can lead to mortality by developing into pulmonary embolism, and cause a heavy burden to individuals and society by deteriorating into post-thrombotic syndrome, characterized by chronic leg pain, swelling, and ulceration [3, 4]. Surgical patients with recognized/unrecognized risk factors are more prone to DVT and more likely to develop complications including pulmonary embolism, postphlebotic syndrome and recurrent DVT [5]. The risk factors for DVT include central venous catheters, mechanical compressions, chronic medical conditions and thrombophilia [6, 7]. After anticoagulant drug withdrawal, DVT is of high risk for recurrence, and for now, ultrasound remains the most useful test for the diagnosis of recurrent DVT [8]. Therefore, understanding the pathobiology of DVT is of equal importance to address the prevention techniques and anticoagulation therapy in clinical studies.

Several microRNAs (miRs) have been validated in patients with VTE for their regulation on messenger RNA in venous thrombosis development [9]. In parallel, a subset of miRs has been identified as potential biomarkers for DVT [10–12]. Catheter-directed techniques are widely applied for thrombus removal for extensive proximal DVT, which requires accurate assessment of thrombus age [13]. Endothelial cells (ECs) and vascular smooth muscle cells (VSMCs) constitute the most essential part of the vessel wall, whose alteration in function remains the leading cause of vascular aging [14, 15]. Milk fat globule-epidermal growth factor 8 (MFG-E8) is a multifunctional glycoprotein which exerts a regulatory role in the intercellular interactions, and evidence in a previous study identified MFG-E8 as a novel and outstanding modulator for vascular aging via targeting at ECs and VSMCs [15]. In addition to that, MFG-E8 is also proved to be a promising biomarker for aging arteries and atherosclerosis [16, 17]. Despite that, evidence supporting the involvement of MFG-E8 in VTE or DVT is lacking.

Several miRs are confirmed to have a certain relationship with cholesterol metabolism in atherosclerosis, such as miR-19b, miR-378, miR-10b, miR-33a, and miR-33b [18]. The role and function of miR-10b expression in cholesterol efflux and atherosclerosis progression were investigated in a previous study [19]. Nevertheless, no study has explored the possible effect of miR-10b in VTE or DVT. In our study, we through online prediction identified the possible interaction between MFG-E8 and miR-10b, and we aimed to explore the possible effect and mechanism of MFG-E8 and

miR-10b in the development of DVT with the expectation to provide a theoretical basis for better understanding the pathobiology of DVT.

Material and methods

Clinical samples

From February 2019 to October 2020, DVT patients ($N = 40$, DVT group) who were pathologically diagnosed with symptoms for more than 21 days and healthy controls ($N = 40$, blank group) were included in the study. The DVT patients included in this study were confirmed with color Doppler ultrasound and CT angiography of lower extremities and any chronic diseases such as hypertension or diabetes mellitus were excluded. The peripheral blood (5 ml) was collected from each subject in both the DVT group and blank group. The experimental design of this study was approved by the ethical committee of Tongji Hospital and abided by the Declaration of Helsinki. Consent was obtained from each of the participants.

DVT model establishment

SD rats (300 ± 20 g) purchased from Hunan SJA Laboratory Animal Co., Ltd. (Hunan, China) were housed in cages at $20\text{--}25^\circ\text{C}$ with humidity of $50\text{--}60\%$. Rats had free access to food and water. Rats were anesthetized with 3% pentobarbital sodium (1 ml/kg) and fixed in a supine position to make a longitudinal incision in the thigh to expose the femoral vein. The femoral vein was clipped by hemostatic forceps to establish the DVT model, as shown in a previous study [20]. One day after the incision was stitched, the edema and the skin of the lower extremity were observed. The rats subjected to DVT model establishment had obvious edema and bruising in the lower extremity. The femoral vein of rats in the sham group was not clipped with hemostatic forceps. All experiments were approved by the ethical committee of Tongji Hospital.

Four days before model establishment, rats were injected with 400 pmol inhibitor-NC (negative control), 400 pmol miR-10b-5p, 400 pmol OE-NC (overexpression negative control) or 400 pmol OE-MFG-E8 through peritoneal injection. All plasmids were purchased from GeneChem (Shanghai, China).

Measurement of thrombus size

After DVT model established for 24 h, rats were anesthetized with 3% pentobarbital sodium (1 ml/kg) in a supine position. The skins of the abdomen were disinfected and an incision of 2–3 cm was made in the original wound. The contents of the abdomen were gently removed and then the

postcava tissues were isolated with the inflammatory hyperplasia tissues around the wound removed to fully expose the intravenous tissue. The postcava and embolus were cut under ligation. The length and weight of the thrombus were recorded. For control, postcava tissues (1–1.5 cm) at the end of the left pulmonary vein were cut in rats only injected with 20 mL of normal saline, from which the length and weight of the tissues were measured (Sartorius BSA224S-CW analytical balance) and the length of the thrombus was measured (Mitutoyo 530-119, Vernier, Caliper, two decimal places). The ratio of weight and length of the thrombus was analyzed. The vascular wall and embolus was isolated and preserved at -80°C .

TUNEL staining

The TUNEL staining kit was purchased from Beyotime (C1098, Beyotime, Shanghai, China). The paraffin section was fixed in 4% paraformaldehyde for 10 min, and subjected to permeabilization with 0.2% Triton-X-100 for 10 min. Then the sections were incubated with blocking solution for 20 min before 50 μl of biotin label buffer was added for incubation of 60 min without light exposure. After that, the sections were incubated with 50 μl of Streptavidin-HRP at room temperature for 30 min and subjected to color development with 0.3 ml of DAB for 5 min. The slices were sealed before observation under a microscope.

H&E staining

The postcava tissues were fixed with 4% paraformaldehyde for 24 h and then washed with PBS and running water before being dehydrated for 12 h and embedded in paraffin. The tissues were sliced at 0.4 mm thickness and baked at 65°C for 2 h. Then the slices were subjected to dewaxing, hematoxylin staining, washing in running water, differentiation with 0.2% acid alcohol, washing in running water, and eosin staining. After staining, the slices were baked in an oven for 30 min, dewaxed, dried and sealed by neutral resins. The formation of a thrombus was observed under a light microscope and photographed.

Cell culture and transfection

Human umbilical vein endothelial cells (HUVECs) were purchased from the ATCC cell bank and cultured with DMEM (11965092, Gibco, New York, USA) containing 10% FBS (16140071, Gibco, New York, USA) at 37°C with 5% CO_2 . The following plasmids were all purchased from GeneChem (Shanghai, China): MFG-E8 overexpression plasmid (OE-MFG-E8), MFG-E8 knockdown plasmid (sh-MFG-E8), negative control for overexpression (OE-NC), negative control for knockdown (sh-NC),

miR-10b-5p mimic plasmid (miR-10b-5p mimic), miR-10b-5p inhibitor plasmid (miR-10b-5p inhibitor) and their negative controls (mimic-NC, inhibitor-NC).

One day before cell transfection, cells were coated into a 60 mm culture disk at the density of 3.0×10^5 cell/disk for cell culture of 24 h before cell incubation with 3 μg of plasmid, Lipofectamine 2000 reagent (11668019, Invitrogen, Calif, USA), Opti-MEM I (31985062, Gibco, New York, USA) and reduced serum medium. Then 8 ng/mL polybrene (TR-1003, Sigma-Aldrich, St. Louis, MO, USA) was added into cells for 48 h of incubation before cells were treated with 250 μM CoCl_2 for 12 h to simulate a hypoxia HUVEC model.

Detection of cell apoptosis

Once cell confluence reached 80%, the cells were collected and counted. Then 1×10^6 cells were washed with pre-cold PBS twice and suspended in $1 \times$ Annexin loading buffer before incubation with 5 μl Annexin-VFITC (Becton Dickinson) at room temperature without light exposure for 10 min. After that, cells were washed with pre-cold PBS and suspended in 100 μl of $1 \times$ Annexin. The cell apoptosis rate was determined using flow cytometry (Guava easyCyte HT from Millipore).

MTT

Cells were collected and adjusted to 1×10^4 cells/ml before cell culture at 37°C in an incubator with 5% CO_2 in 96-well plates. After cell culture for respectively 24 h, 48 h and 72 h, 20 μl of 5 mg/ml MTT was added to cells for incubation at 37°C with 5% CO_2 . Four hours later, the excessive liquid was removed and cells were mixed with 200 μl of DMSO. The optical density of cells in each well was measured using a microplate reader at 490 nm.

Cell scratch assay

Cells (1×10^5) were seeded into a 12-well plate and once cell confluency reached 100%, a 10 μl pipette tip was used to make a scratch on the well. Then cells in the plate were washed with DPBS (14190250, Gibco, New York, USA) 3 times and cultured in DMEM containing 2% FBS. Cells under the same field after cell culture for respectively 0 h and 24 h were observed under an Olympus inverted microscope to record the cell scratch changes. Migration rate of cells = (scratch at 0 h – scratch at 24 h) / scratch at 0 h. Three duplicates were set for each group.

Tube formation assay

Matrigel (50 μl , BD Bioscience, USA) was coated in 1 96-well plate for incubation at 37°C for

0.5 h. Cells and HUVECs were centrifuged at 1000 rpm for 5 min, after which HUVECs were resuspended in the supernatant of cells. Then the HUVECs (4×10^4 cells/well) were seeded into the Matrigel for incubation at 37°C for 6 h with 5% CO₂. Tube formation in HUVECs was observed under an inverted microscope (CKX40, Olympus, New York, USA).

Western blot

The collected cells or tissues were treated with cell lysis buffer before the concentration of total protein was determined using a BCA protein kit (23227, Thermo Fisher, USA). The proteins were diluted with 5 × loading buffer and separated in 12% separating gel for 90 min. Then PBS containing 5% (w/v) skimmed milk powder was used to incubate with proteins at room temperature for 1 h to terminate unspecific reactions. Subsequently, the proteins were incubated with the primary antibodies MFG-E8 (1 : 500, ab200649, abcam, Cambridge, UK), JAK (1 : 500, ab133666, abcam, Cambridge, UK), p-JAK (1 : 500, ab138005, abcam, Cambridge, UK), STAT3 (1 : 500, ab68153, abcam, Cambridge, UK), p-STAT3 (1 : 500, ab267373, abcam, Cambridge, UK) and GAPDH (1 : 500, ab9485, abcam, Cambridge, UK) at 4°C overnight before being washed and incubated with secondary antibody (1 : 500, ab150077, abcam, Cambridge, UK) at room temperature for 1 h. The bands were analyzed and photographed using the BioSpectrum Imaging System (UVP, USA).

Luciferase reporter gene assay

StarBase (<http://starbase.sysu.edu.cn/index.php>) predicted the binding sites of miR-10b-5p with MFG-E8 and the mutant sites were designed accordingly. The wide sequence (WT-MFG-E8) and mutant sequence (MT-MFG-E8) of MFG-E8 were cloned into psiCHECK-2 (C8011, Promega, Madison, Wisconsin, USA) in the downstream coding re-

gion of renal luciferase. To verify the effect of miR-10b-5p, the psiCHECK plasmid and miR-10b-5p mimic or negative control were co-transfected into HK-2 cells. After cell transfection for 48 h, the activities of renal luciferase were analyzed using the Dual-Glo luciferase analysis system (Promega) and standardized using firefly luciferase activity as a control.

RT-qPCR

Tissues or cells were dissolved in 1 mL of Trizol (Thermo Fisher Scientific, MA, USA) for extraction of total RNA based on the kit instructions. The extracted total RNA was reversed transcribed into cDNA using M-MLV reverse transcriptase and random primers. The PCR reaction system was prepared based on instructions on the Premix Ex Taq II kit (Takara, Dalian, China) and the conditions for the PCR reaction were set. The ABI7500 PCR instrument (Applied Biosystems, Shanghai, China) was used for RT-PCR, using GAPDH as an internal control. Relative expression of the target gene was analyzed using the 2^{-ΔΔCt} method [21]: $\Delta\Delta Ct = [Ct_{(target\ gene)} - Ct_{(internal\ control)}]_{experimental\ group} - [Ct_{(target\ gene)} - Ct_{(internal\ control)}]_{control\ group}$. The primer sequences of each target gene are listed in Table I.

Statistical analysis

Data were analyzed using GraphPad Prism 8.0. Quantitative data were expressed as mean ± SEM and subjected to Shapiro-Wilk testing for normal distribution. One-way analysis of variance (ANOVA) was used for data analysis among more than 3 groups. The correlation was assessed using Pearson analysis. Comparison between two groups was analyzed using Student's t test. The Bonferroni test was used as a post hoc test. *P* < 0.05 was considered to have statistical significance.

Results

Elevated expression of miR-10b-5p and decreased MFG-E8 expression in peripheral blood of DVT patients

The expression of miR-10b-5p and MFG-E8 in the peripheral blood of DVT patients was detected by RT-qPCR and Western blot. The results showed that DVT patients had higher expression of miR-10b-5p and lower MFG-E8 expression (Figures 1 A, B, *p* < 0.01), compared with those in the blank group. Pearson coefficient analyzing the correlation of miR-10b-5p and MFG-E8 showed that miR-10b-5p expression in DVT patients was negatively correlated with that of MFG-E8 (Figure 1 C, *p* < 0.01). Taken together, these results support the involvement of miR-10b-5p and MFG-E8 in the development of DVT.

Table I. Primer sequences used for reverse transcription polymerase chain reaction

Name of primer	Sequences (5'-3')
MFG-E8-F	CTCCACTCAAACCTCGCCCAT
MFG-E8-R	ATGGGCCTCCTTTGCAATCA
miR-10b-5p-F	gTGTTTAAGCCAAGATG
miR-10b-5p-R	TGGTGTCGTGGAGTCG
U6-F	CTCGCTTCGGCAGCAC
U6-R	AACGCTTCACGAATTTGCGT
GAPDH-F	GTTGGCTGCTCAGAAAAGG
GAPDH-R	GGGGAGATTCAGTGTGGTGG

F – forward primer, *R* – reverse primer.

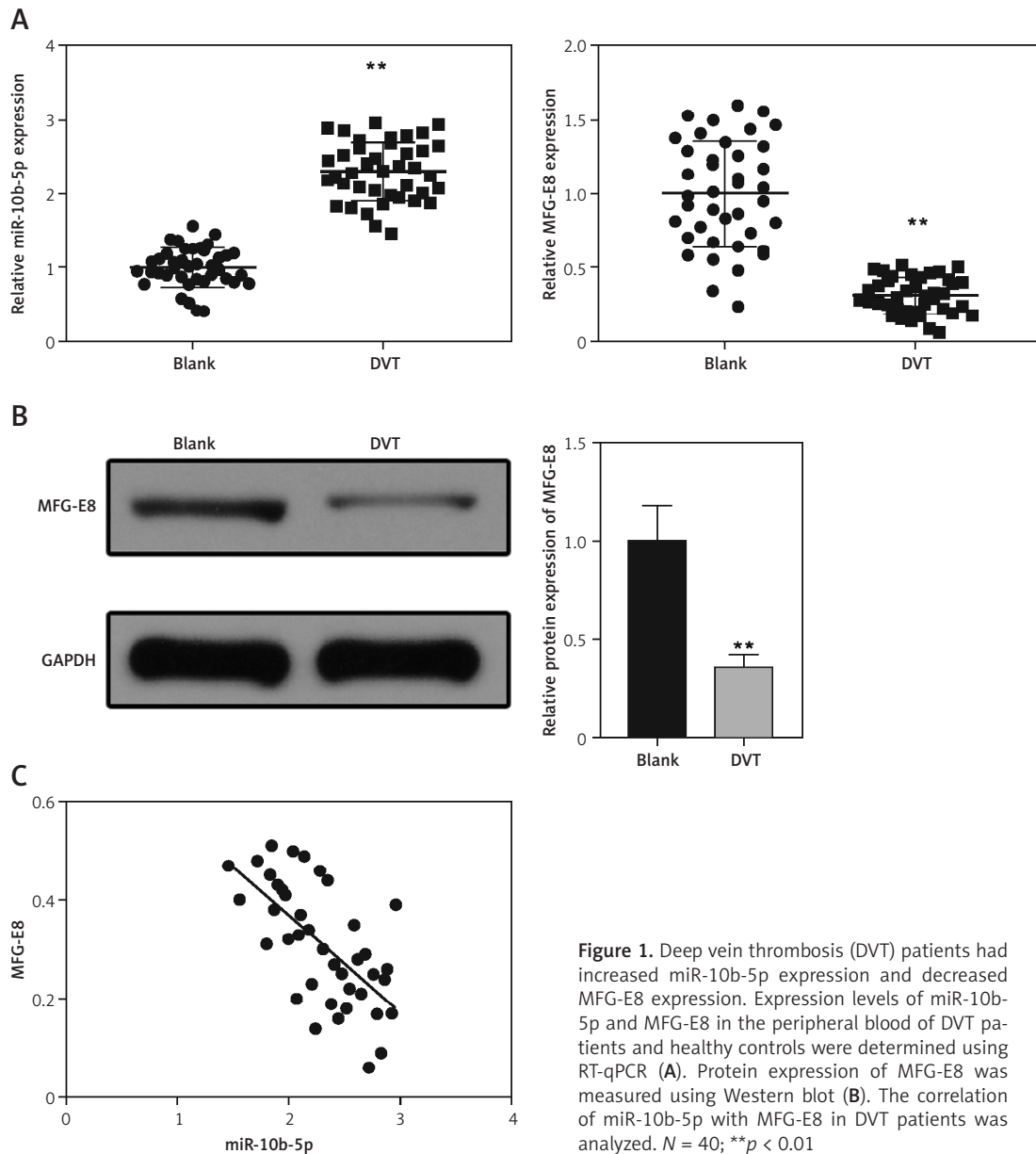


Figure 1. Deep vein thrombosis (DVT) patients had increased miR-10b-5p expression and decreased MFG-E8 expression. Expression levels of miR-10b-5p and MFG-E8 in the peripheral blood of DVT patients and healthy controls were determined using RT-qPCR (A). Protein expression of MFG-E8 was measured using Western blot (B). The correlation of miR-10b-5p with MFG-E8 in DVT patients was analyzed. $N = 40$; $**p < 0.01$

Inhibition of miR-10b-5p or overexpression of MFG-E8 can attenuate DVT in rat models

To verify the possible effect of miR-10b-5p or MFG-E8 in DVT, we established a DVT rat model to measure the miR-10b-5p and MFG-E8 expression. Compared with the sham group, rats in the Model group had increased miR-10b-5p and decreased MFG-E8 expression in the intravenous tissues (Figure 2 A, B, $p < 0.01$). Then DVT rats were injected with the miR-10b-5p inhibitor plasmid (miR-10b-5p inhibitor) or MFG-E8 overexpression plasmid (OE-MFG-E8) through tail intravenous injection. To verify the plasmid transfection efficiency, the expression levels of miR-10b-5p and MFG-E8 in DVT rats were measured. Compared with those injected with inhibitor-NC, DVT rats injected with miR-10b-5p inhibitor had decreased miR-10b-5p

expression, while compared with those injected with OE-NC, DVT rats injected with OE-MFG-E8 had elevated expression of MFG-E8 (Figure 2 C, D, $p < 0.01$). Those results showed that miR-10b-5p inhibition or MFG-E8 overexpression was successfully achieved in DVT rats. Measurement of thrombosis-related symptoms showed that rats in the Model group, miR-10b-5p inhibitor group and OE-MFG-E8 group had edema and venous thrombus in the postcava (Figure 2 E), compared with the sham group, which indicates that DVT rat models were successfully established in the model group. To quantify the venous thrombus, the length and weight of the thrombus were measured, which showed that compared with the Model group, rats in the miR-10b-5p inhibitor group and OE-MFG-E8 group had decreased thrombus length

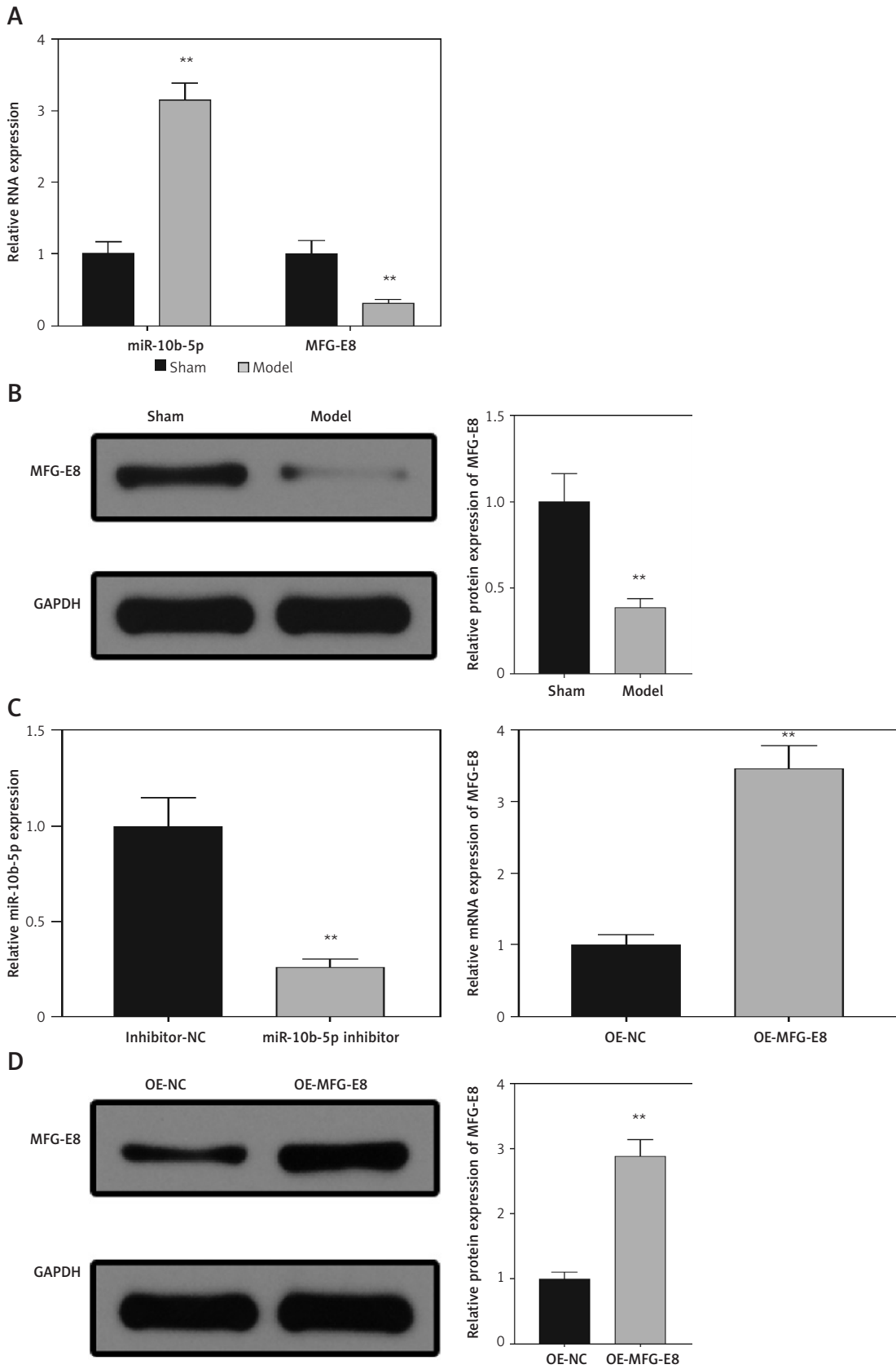


Figure 2. Rat tail intravenous injection of miR-10b-5p inhibition plasmid or MFG-E8 overexpression plasmid could attenuate deep vein thrombosis (DVT) progression. Rats were subjected to tail intravenous injection of miR-10b-5p inhibition plasmid or MFG-E8 overexpression plasmid before DVT model establishment. The RNA and protein expression levels of miR-10b-5p and MFG-E8 were detected by RT-qPCR (A, C) and Western blot (B, D). $N = 6$; *compared with sham group, $p < 0.05$, **compared with sham group, $p < 0.01$; #compared with Model group, $p < 0.05$, ##compared with model group, $p < 0.01$

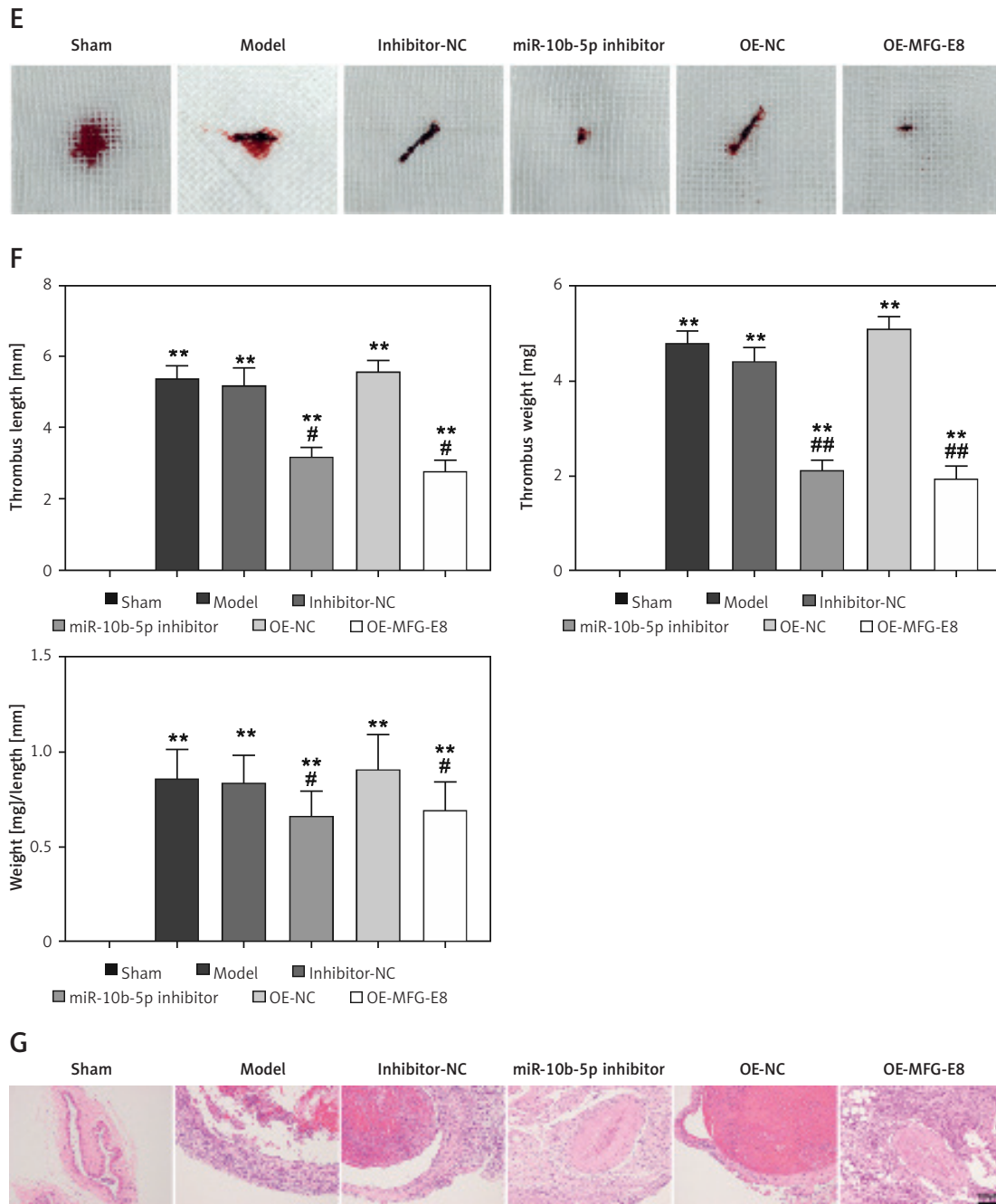


Figure 2. Cont. Length of venous length (E). Measurement of thrombus length, weight, and weight/length ratio of thrombus (F). Venous morphologies in each group were observed after H&E staining (G). TUNEL staining detected the apoptosis of vascular endothelial cells (H). $N = 6$; *compared with sham group, $p < 0.05$, **compared with sham group, $p < 0.01$; #compared with Model group, $p < 0.05$, ##compared with model group, $p < 0.01$

H

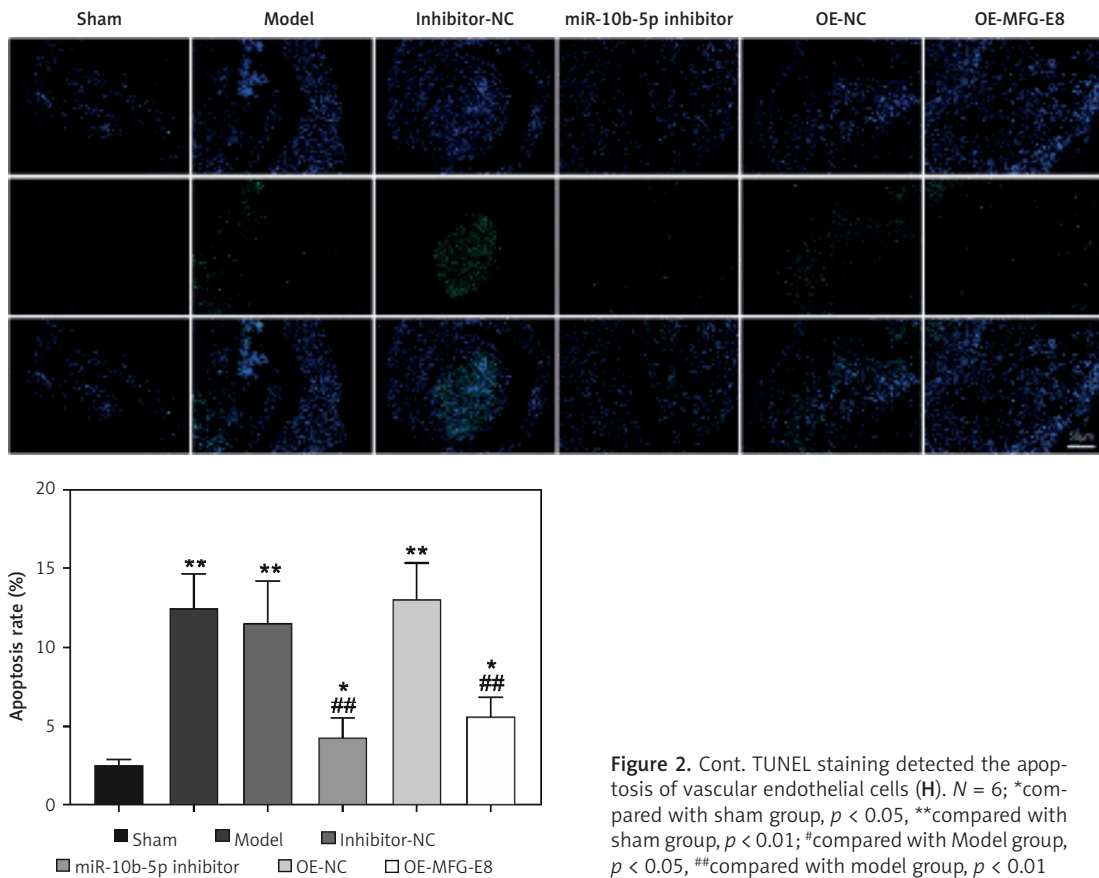


Figure 2. Cont. TUNEL staining detected the apoptosis of vascular endothelial cells (H). $N = 6$; *compared with sham group, $p < 0.05$, **compared with sham group, $p < 0.01$; #compared with Model group, $p < 0.05$, ##compared with model group, $p < 0.01$

and weight, as well as a lower weight/length ratio of the thrombus (Figure 2 F, $p < 0.01$).

Intravenous tissue of rats in each group was analyzed after H&E staining. The observation showed that no venous thrombus was observed in the sham group, the Model group had complete venous thrombosis, while the miR-10b-5p inhibitor group and OE-MFG-E8 group had partial venous thrombosis (Figure 2 G). TUNEL staining detecting the apoptosis of vascular endothelial cells demonstrated that compared with the sham group, Model group had higher cell apoptosis, while compared with the Model group, the apoptosis of the miR-10b-5p inhibitor group and OE-MFG-E8 group was lower (Figure 2 H, $p < 0.01$). Taken together, inhibition of miR-10b-5p or overexpression of MFG-E8 can attenuate the progression of DVT in rats.

miR-10b-5p targets and negatively regulates MFG-E8 expression

Considering the negative correlation of miR-10b-5p with MFG-E8 in DVT and the effect of miR-10b-5p and MFG-E8 on DVT rat models, we hypothesized that there may be possible interaction between the two parameters. StarBase database demonstrated the direct binding sites

of miR-10b-5p with MFG-E8. The binding site and mutant site are shown in Figure 3 A. The mutant sequence (MT-MFG-E8) and wide sequence (WT-MFG-E8) of MFG-E8 were designed and co-transfected with miR-10b-5p mimic or mimic-NC into HK-2 cells. After that, the fluorescence intensity of cells in each group was measured. Compared with the mimic-NC group, co-transfection of WT-MFG-E8 with the miR-10b-5p mimic led to suppressed fluorescent intensity (Figure 3 B, $p < 0.01$), while no significant difference was observed for co-transfection of MT-MFG-E8 with miR-10b-5p mimic ($p > 0.05$). These results show that miR-10b-5p can specifically bind with MFG-E8.

To verify the regulatory effect of miR-10b-5p on MFG-E8, HUVECs were transfected with miR-10b-5p mimic or miR-10b-5p inhibitor before the expression of MFG-E8 in cells was determined. RT-qPCR showed that compared with the mimic-NC group the expression of miR-10b-5p in the miR-10b-5p mimic group was enhanced while compared with the inhibitor-NC group, the expression of miR-10b-5p in the miR-10b-5p inhibitor group was suppressed (Figure 3 C, $p < 0.01$). RT-qPCR and Western blot detecting MFG-E8 expression showed that the miR-10b-5p mimic

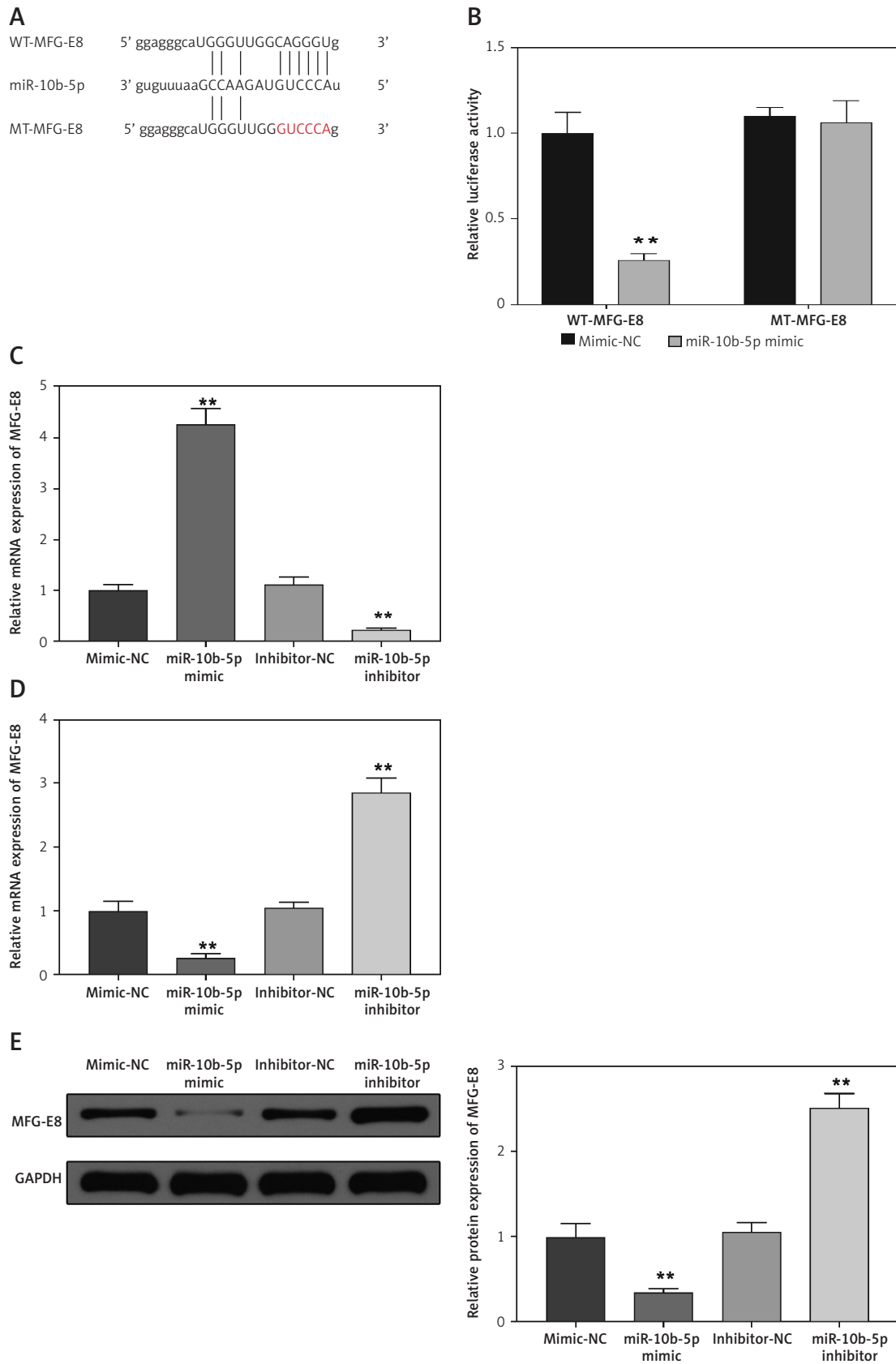


Figure 3. miR-10b-5p negatively regulates MFG-E8 expression. Binding sites of miR-10b-5p with MFG-E8 were predicted by StarBase and the mutant sites were designed accordingly (A). Interaction of miR-10b-5p with MFG-E8 was verified by dual luciferase reporter gene assay (B). RNA expression levels of miR-10b-5p and MFG-E8 were determined by RT-qPCR (C, D). Protein expression of MFG-E8 was detected by Western blot (E). $N = 3$, $**p < 0.01$

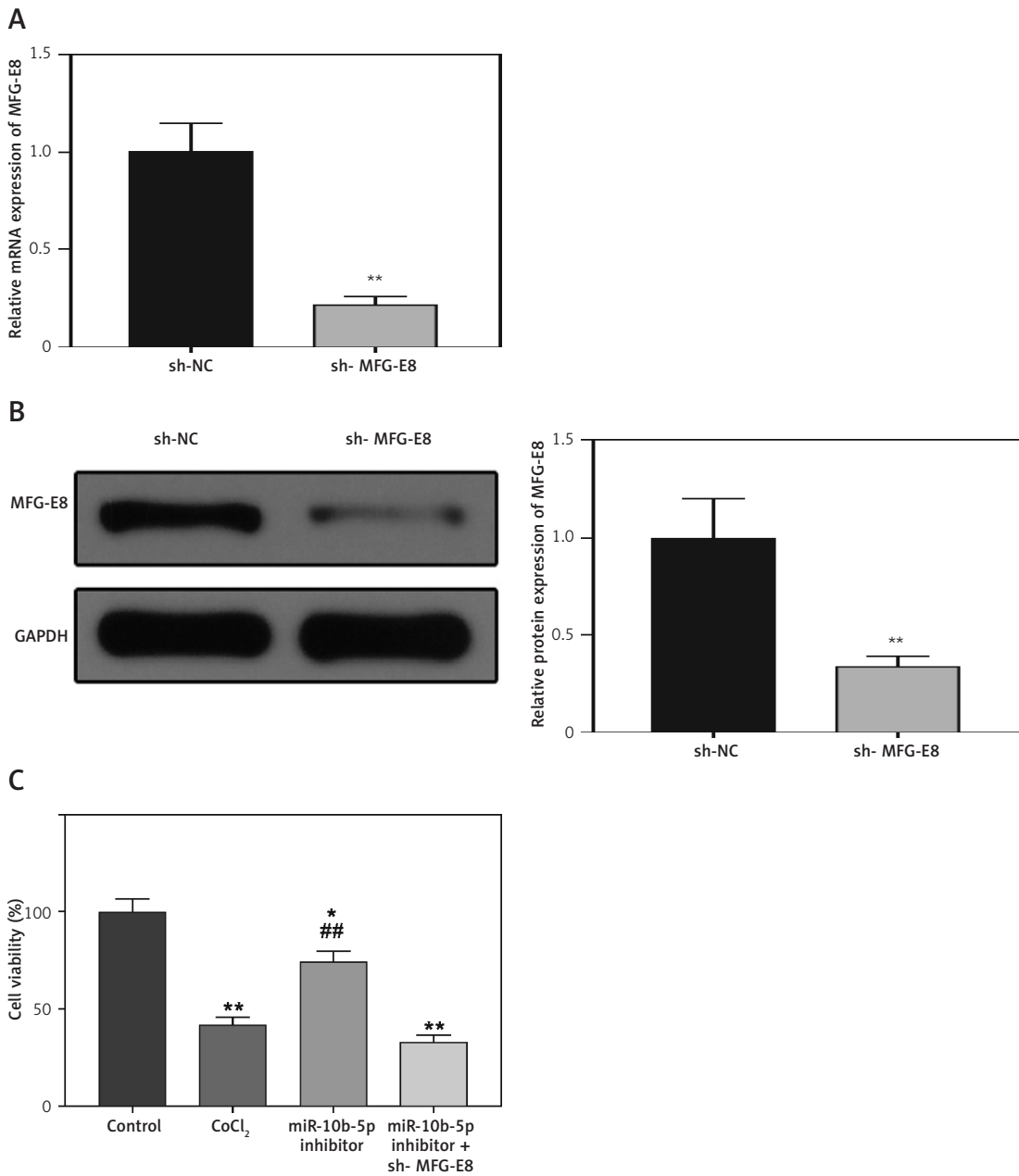


Figure 4. miR-10b-5p promotes human umbilical vein endothelial cells (HUVEC) apoptosis through suppressing MFG-E8 expression. miR-10b-5p or MFG-E8 was transfected into HUVECs before CoCl₂ treatment. RT-qPCR (A) and Western blot (B) were applied to verify the transfection efficiency; (C) MTT assay to detect cell viability

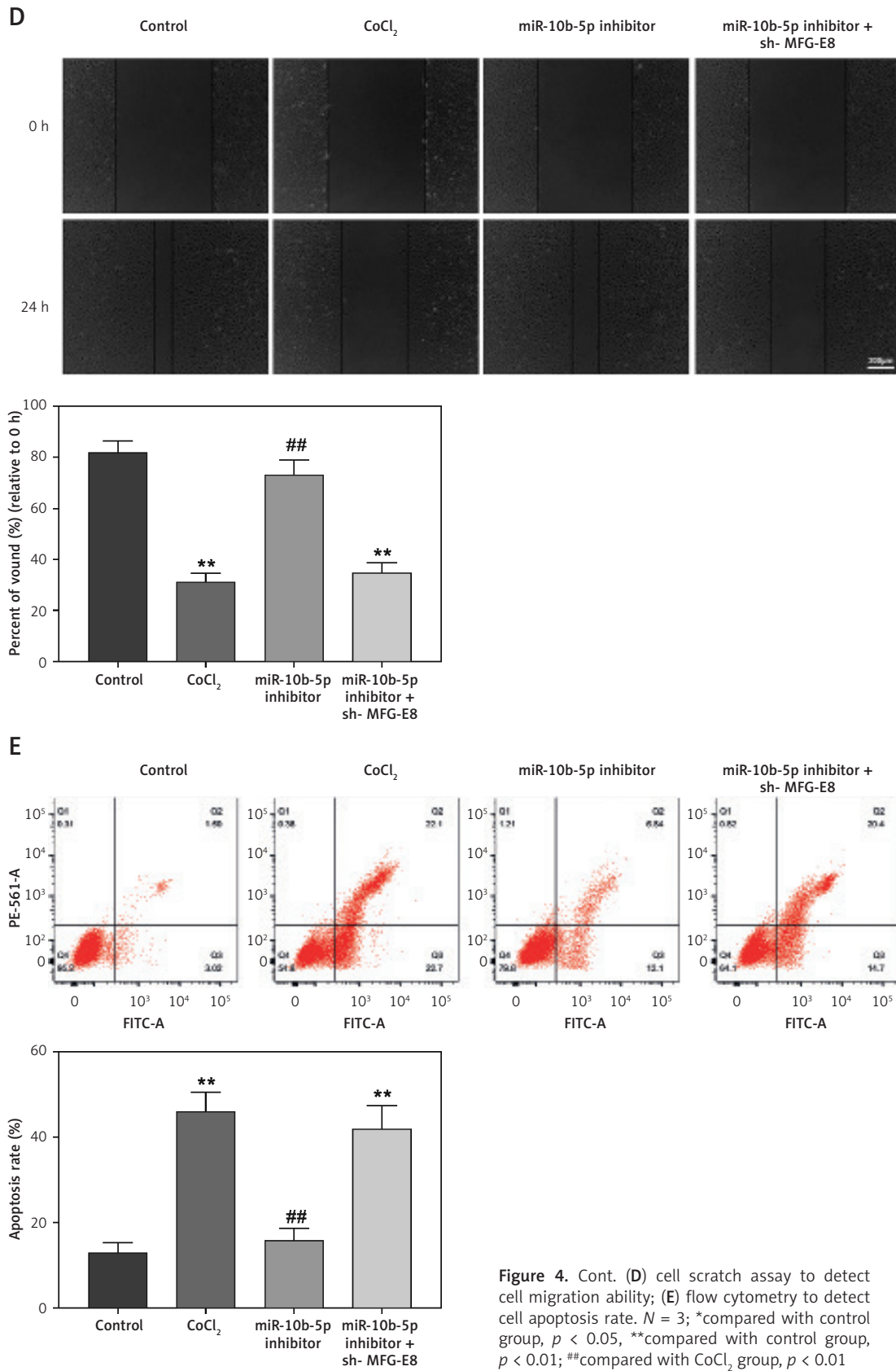


Figure 4. Cont. (D) cell scratch assay to detect cell migration ability; (E) flow cytometry to detect cell apoptosis rate. $N = 3$; *compared with control group, $p < 0.05$, **compared with control group, $p < 0.01$; ##compared with CoCl₂ group, $p < 0.01$

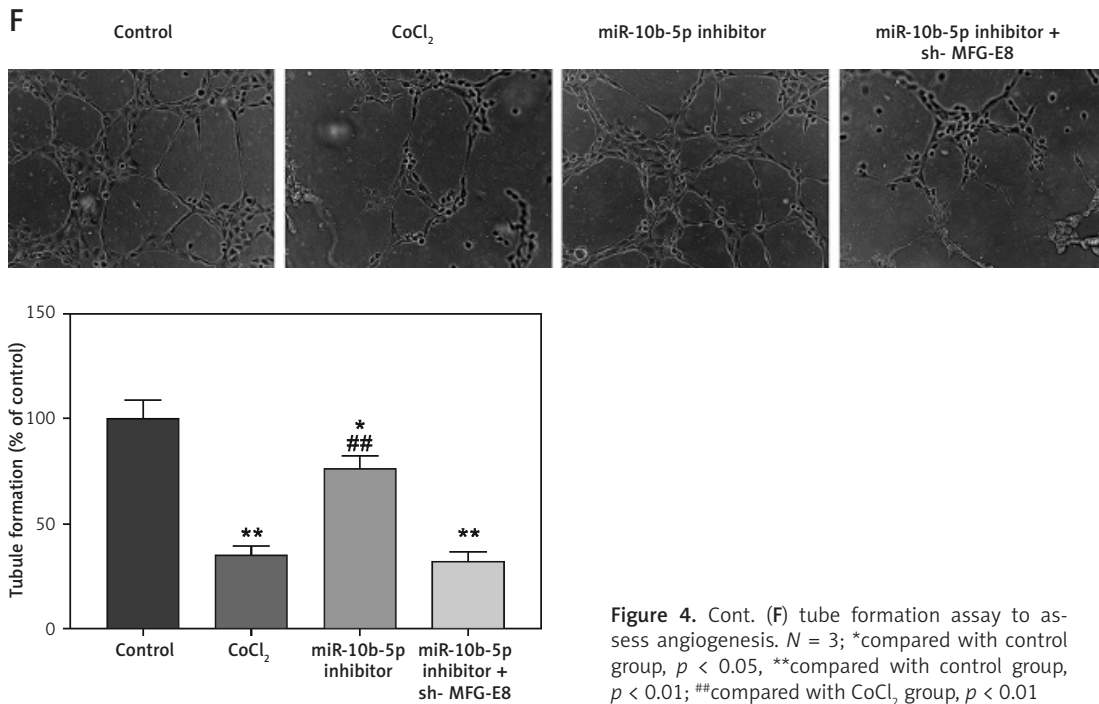


Figure 4. Cont. (F) tube formation assay to assess angiogenesis. $N = 3$; *compared with control group, $p < 0.05$, **compared with control group, $p < 0.01$; ##compared with CoCl₂ group, $p < 0.01$

group had suppressed MFG-E8 expression when compared with the mimic-NC group, while the miR-10b-5p inhibitor group had elevated expression of MFG-E8 when compared with inhibitor-NC (Figure 3 D, E, $p < 0.01$). Taken together, miR-10b-5p can target and negatively regulate MFG-E8 expression.

miR-10b-5p promotes HUVEC apoptosis through suppressing MFG-E8 expression

To clarify whether miR-10b-5p regulates apoptosis of HUVECs through regulating MFG-E8 expression, cell transfection was performed in HUVECs. The detection of MFG-E8 expression showed that compared with the sh-NC group, the expression of MFG-E8 in the sh-MFG-E8 group was suppressed (Figure 4 A, B, $p < 0.01$), indicating that MFG-E8 was suppressed in HUVECs. To simulate a hypoxia injury cell model, HUVECs were treated with CoCl₂ for 12 h. Measurement showed that compared with the control group, cells in the CoCl₂ group had suppressed cell activities (Figure 4 C, $p < 0.01$), inhibited cell migration (Figure 4 D, $p < 0.01$), lower tube formation ability (Figure 4 F, $p < 0.01$) and enhanced cell apoptosis (Figure 4 E, $p < 0.01$). These results showed that CoCl₂ successfully induced HUVEC injury.

Compared with the CoCl₂ group, cells in the miR-10b-5p inhibitor group had increased cell viability, migration, invasion and tube formation abilities as well as suppressed cell apoptosis. Compared with the miR-10b-5p inhibitor group, the miR-10b-5p inhibitor + sh-MFG-E8 group had suppressed cell viability, migration, invasion and tube

formation abilities, and additionally enhanced cell apoptosis (Figure 4 C–F, $p < 0.01$). Taken together, inhibition of miR-10b-5p expression can attenuate CoCl₂-induced cell injury in HUVECs.

miR-10b-5p suppresses MFG-E8 to activate the JAK/STAT signal pathway

Evidence in previous studies showed that DVT can promote IL-6 expression to trigger a inflammatory response [10, 22]. To ascertain the role of miR-10b-5p and MFG-E8 in regulating the IL-6 related signal pathway, we measured the expression levels of JAK/STAT signal pathway related proteins. Then results showed that compared with the sham group, rats in the Model group had a higher p-JAK/JAK ratio and p-STAT3/STAT3 ratio in postcava tissues, while compared with the Model group, the p-JAK/JAK ratio and p-STAT3/STAT3 ratio in the miR-10b-5p inhibitor group and OE-MFG-E8 group were suppressed (Figure 5 A, $p < 0.01$), indicating that DVT activates the JAK/STAT signal pathway. MFG-E8 overexpression or inhibition of miR-10b-5p suppresses the DVT-activated JAK/STAT signal pathway.

The expression levels of p-JAK/STAT related proteins in HUVECs were also measured and the results showed that compared with the control group, HUVECs in the CoCl₂ group had an increased p-JAK/JAK ratio and p-STAT3/STAT3 ratio, while compared with the CoCl₂ group, cells in the miR-10b-5p inhibitor group had a decreased p-JAK/JAK ratio and p-STAT3/STAT3 ratio. Additionally, compared with the miR-10b-5p inhibitor group, the p-JAK/JAK ratio and p-STAT3/STAT3 ra-

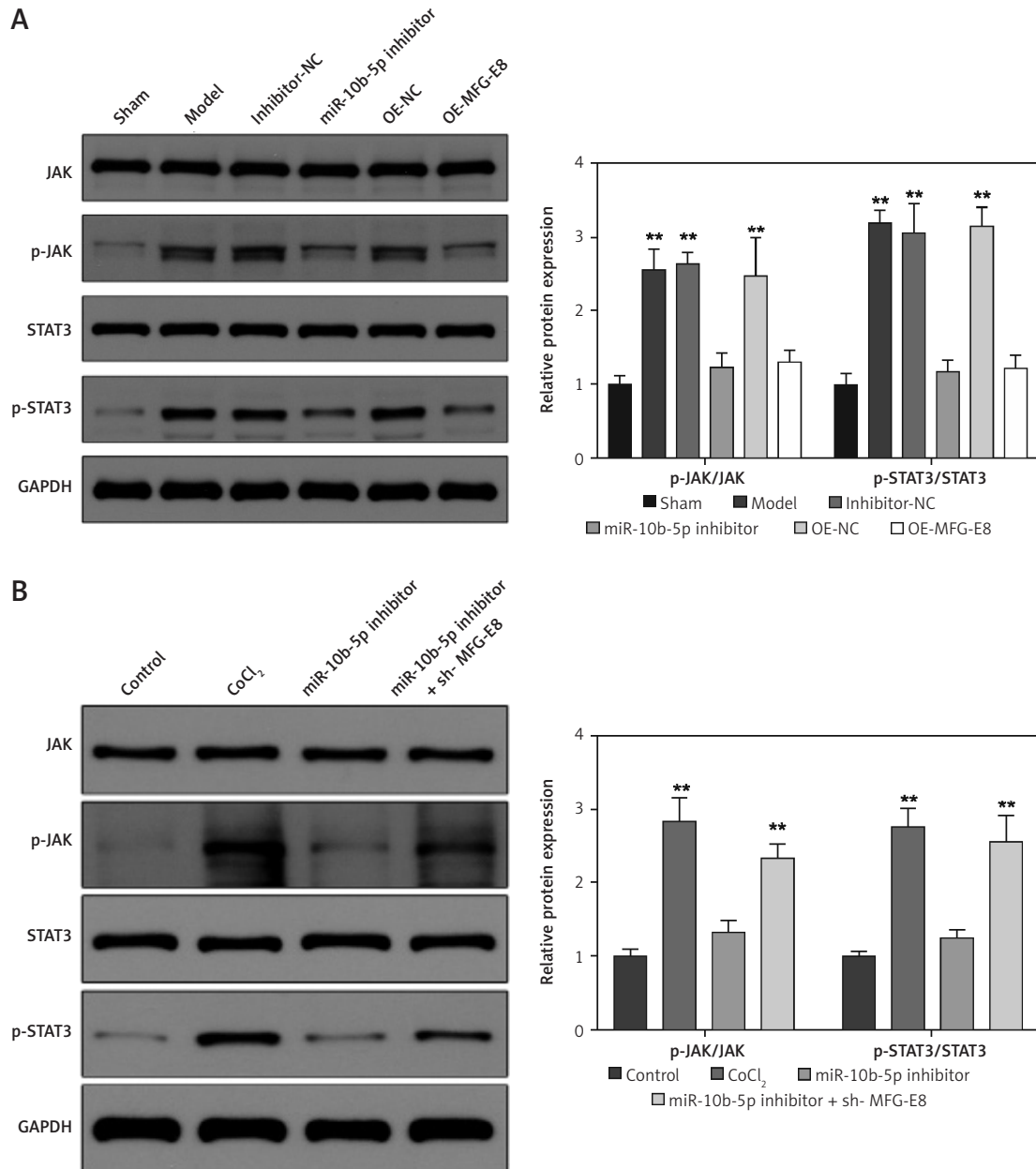


Figure 5. Suppression of miR-10b-5p in human umbilical vein endothelial cells (HUVECs) can suppress deep vein thrombosis (DVT) activated JAK/STAT signal pathway. Expression of JAK/STAT signal pathway related proteins in rats (A) and HUVECs (B) was detected by Western blot. $**p < 0.01$

tion in the miR-10b-5p inhibitor + sh-MFG-E8 group were elevated (Figure 5 B, $p < 0.01$). Taken together, DVT can activate the JAK/STAT signal pathway, while suppression of miR-10b-5p in HUVECs can suppress activation of the JAK/STAT signal pathway through increasing MFG-E8 expression.

Discussion

Emerging evidence has highlighted the importance of the possible role and mechanism of certain miRs in the formation of venous thrombosis [23]. The implication of miRs in development of venous thrombosis and DVT has been well docu-

mented in previous studies [10, 24]. In our current study, we identified that miR-10b-5p can regulate the progression of DVT through targeting MFG-E8 and the JAK/STAT signal pathway.

miR-10b-5p has long been reported as a biomarker for various tumors, including breast cancer [25], hepatocellular carcinoma [26], and colorectal cancer [27]. In the current study, measurement of expression of miR-10b-5p and MFG-E8 in clinical peripheral blood of DVT patients and in the DVT rat models consistently supported the implication of both miR-10b-5p and MFG-E8 in DVT progression. In agreement with our results, in a study researching atherosclerosis, miR-10b-3p was found

to bind with SMILR and its expression was down-regulated in the serum of atherosclerosis patients and in atherosclerosis cell models induced by ox-LDL [28]. Additionally, miR-10b-5p, serving as an exosomal microRNA, was also found to have a certain relationship with angiogenesis-related biological functions and intracranial atherosclerotic disease related angiogenic factors [29]. MFG-E8 is generally reported for its regulation in biological functions of tumor cells, including cell inflammation [30], microglial polarization [31], as well as for its potential to serve as a prognosis biomarker for cancers [32, 33]. Nevertheless, in our study we found a suppressed expression level of MFG-E8 in DVT patients, which highlighted the potential for its involvement in DVT progression.

To fully address the possible role and possible mechanism of miR-10b-5p and MFG-E8 in DVT, we measured the effect of miR-10b-5p and MFG-E8 on thrombus formation and endothelial apoptosis by genetically manipulating its expression in gain and loss-of-function experiments. The results showed that suppression of miR-10b-5p or overexpression of MFG-E8 can attenuate the DVT progression in rat models, which further confirmed the potential effect of miR-10b-5p and MFG-E8 in DVT progression. In this regard, we speculated that there may be a certain interaction between miR-10b-5p and MFG-E8. Unsurprisingly, online prediction by StarBase software and dual luciferase reporter gene assay showed that MFG-E8 is a downstream target of miR-10b-5p, which prompted us to verify the possible interaction of MFG-E8 and miR-10b-5p in Co-Cl₂-treated HUVECs so as to simulate hypoxia cell models. The detection of cell biological function and apoptosis showed that miR-10b-5p promoted the apoptosis of HUVECs through suppressing the expression of MFG-E8. The regulation of miR-10 on endothelial cells has been reported in a previous study which identified that miR-10b was up-regulated in the tumor vasculature in response to vascular endothelial growth factor (VEGF) stimulation [34], which was consistent with the observation in our study that miR-10b-5p was highly expressed in both DVT patients and rat models. Endothelial cell migration and metastasis are essential for angiogenesis and DVT [35, 36]. The measurement on HUVECs in this study supported the regulatory role of miR-10b-5p in cell biological function of HUVECs. MFG-E8 is often reported for its protective effect against several inflammatory diseases, including ischemia-reperfusion injury and sepsis [37–39], while the results in this study provide a new perspective to explore the possible regulation of MFG-E8 in thrombus-related diseases.

Several classic signaling pathways have been shown to participate in thrombosis, including the

Nrf2/HO-1 signaling pathway [40], nPKC δ /Akt signaling pathway [41] and TLR-4/NF- κ B inflammatory signaling pathway [42]. For the treatment of hematologic malignancies and rheumatological disorders, JAK kinase inhibitors have been proved to have certain efficiency, while concerns have also been raised for high risk of thromboembolic complications, including DVT and pulmonary embolism [43]. Additionally, a review summarized that the formation of venous thrombosis has a certain relationship with altered expression of molecules in the JAK/STAT signaling pathway [44]. Therefore in our cellular experiments, we further determined the ratio of p-JAK/JAK and p-STAT3/STAT3 to assess the activation of the JAK/STAT signaling pathway. The results were consistent with a previous study showing that miR-10b-5p can activate the JAK/STAT signal pathway by suppressing the expression of MFG-E8.

There are several limitations that should be borne in mind when interpreting this study. First of all, the miR-10b-5p/MFG-E8 axis was verified in DVT progression, but DVT is a multifactor disease and associated with a variety of complications. Therefore, the exact mechanism of DVT is far from being understood, and more experiments are necessary. In addition to that, we only detected the expression of miR-10b-5p and MFG-E8 at a clinical level; further validation is required before any of these basic experimental results can be applied as potential therapeutic targets in the clinical treatment of thrombosis. In conclusion, we established that both miR-10b-5p and MFG-E8 were involved in the development of DVT. Specifically, miR-10b-5p can suppress MFG-E8 expression to promote cell apoptosis of endothelial cells and activate the JAK/STAT signaling pathway, therefore aggravating DVT progression.

Acknowledgments

The study was supported by the grant from the National Natural Science Foundation of China (Grant No. 81973992).

Conflict of interests

The authors declare no conflict of interests.

References

1. Bandyopadhyay G, Roy SB, Haldar S, Bhattacharya R. Deep vein thrombosis. *J Indian Med Assoc* 2010; 108: 866-7.
2. Di Nisio M, van Es N, Buller HR. Deep vein thrombosis and pulmonary embolism. *Lancet* 2016; 388: 3060-73.
3. Fras Z, Trsan J, Banach M. On the present and future role of Lp-PLA(2) in atherosclerosis-related cardiovascular risk prediction and management. *Arch Med Sci* 2021; 17: 954-64.
4. Rys RN, Blostein MD, Lemarie CA. Deep vein thrombosis induced by stasis in mice monitored by high frequency ultrasonography. *J Vis Exp* 2018; 134: 57392.

5. Niranjan A, Agarwal N, Agarwal T, Agarwal M. Deep vein thrombosis: review and update. *J Indian Med Assoc* 2010; 108: 248-51.
6. Culler K, Eiswirth P, Donaldson J, Green J, Rajeswaran S. Deep vein thrombosis due to fecal impaction. *J Pediatr Hematol Oncol* 2020; 42: e772-e4.
7. Jaffray J, Young G. Deep vein thrombosis in pediatric patients. *Pediatr Blood Cancer* 2018; 65: doi: 10.1002/pbc.26881.
8. Maufus M, Elias A, Barrellier MT, Pernod G, French Society for Vascular Medicine. Diagnosis of deep vein thrombosis recurrence: Ultrasound criteria. *Thromb Res* 2018; 161: 78-83.
9. Gabler J, Basilio J, Steinbrecher O, Kollars M, Kyrle PA, Eichinger S. MicroRNA Signatures in Plasma of Patients With Venous Thrombosis: A Preliminary Report. *Am J Med Sci* 2021; 361: 509-16.
10. Ou M, Hao S, Chen J, Zhao S, Cui S, Tu J. Downregulation of interleukin-6 and C-reactive protein underlies a novel inhibitory role of microRNA-136-5p in acute lower extremity deep vein thrombosis. *Aging (Albany NY)* 2020; 12: 21076-90.
11. Wang X, Sundquist K, Elf JL, et al. Diagnostic potential of plasma microRNA signatures in patients with deep-vein thrombosis. *Thromb Haemost* 2016; 116: 328-36.
12. Zhang W, Chen P, Zong H, Ding Y, Yan R. MiR-143-3p targets ATG2B to inhibit autophagy and promote endothelial progenitor cells tube formation in deep vein thrombosis. *Tissue Cell* 2020; 67: 101453.
13. Dharmarajah B, Sounderajah V, Rowland SP, Leen EL, Davies AH. Aging techniques for deep vein thrombosis: a systematic review. *Phlebology* 2015; 30: 77-84.
14. Carresi C, Mollace R, Macri R, et al. Oxidative stress triggers defective autophagy in endothelial cells: role in atherothrombosis development. *Antioxidants (Basel)* 2021; 10: 387.
15. Ni YQ, Zhan JK, Liu YS. Roles and mechanisms of MFG-E8 in vascular aging-related diseases. *Ageing Res Rev* 2020; 64: 101176.
16. Chiang HY, Chu PH, Lee TH. MFG-E8 mediates arterial aging by promoting the proinflammatory phenotype of vascular smooth muscle cells. *J Biomed Sci* 2019; 26: 61.
17. Zhao H, Zhang H, Qin X. Agerelated differences in serum MFG-E8, TGFbeta1 and correlation to the severity of atherosclerosis determined by ultrasound. *Mol Med Rep* 2017; 16: 9741-8.
18. Shao D, Lian Z, Di Y, et al. Dietary compounds have potential in controlling atherosclerosis by modulating macrophage cholesterol metabolism and inflammation via miRNA. *NPJ Sci Food* 2018; 2: 13.
19. Wang D, Wang W, Lin W, et al. Apoptotic cell induction of miR-10b in macrophages contributes to advanced atherosclerosis progression in ApoE^{-/-} mice. *Cardiovasc Res* 2018; 114: 1794-805.
20. Bao CX, Zhang DX, Wang NN, Zhu XK, Zhao Q, Sun XL. MicroRNA-335-5p suppresses lower extremity deep venous thrombosis by targeted inhibition of PAI-1 via the TLR4 signaling pathway. *J Cell Biochem* 2018; 119: 4692-710.
21. Burja B, Kuret T, Janko T, et al. Olive leaf extract attenuates inflammatory activation and DNA damage in human arterial endothelial cells. *Front Cardiovasc Med* 2019; 6: 56.
22. Zhang Y, Zhang Z, Wei R, et al. IL (Interleukin)-6 contributes to deep vein thrombosis and is negatively regulated by miR-338-5p. *Arterioscler Thromb Vasc Biol* 2020; 40: 323-34.
23. Ten Cate H. MicroRNA and venous thrombosis. *Thromb Haemost* 2016; 116: 205.
24. Zhang Y, Miao X, Zhang Z, et al. miR-374b-5p is increased in deep vein thrombosis and negatively targets IL-10. *J Mol Cell Cardiol* 2020; 144: 97-108.
25. Wang J, Yan Y, Zhang Z, Li Y. Role of miR-10b-5p in the prognosis of breast cancer. *PeerJ* 2019; 7: e7728.
26. Cho HJ, Eun JW, Baek GO, et al. Serum exosomal microRNA, miR-10b-5p, as a potential diagnostic biomarker for early-stage hepatocellular carcinoma. *J Clin Med* 2020; 9: 281.
27. Lu C, Jiang W, Hui B, et al. The circ_0021977/miR-10b-5p/P21 and P53 regulatory axis suppresses proliferation, migration, and invasion in colorectal cancer. *J Cell Physiol* 2020; 235: 2273-85.
28. Li H, Pan Z, Chen Q, Yang Z, Zhang D. SMILR Aggravates the progression of atherosclerosis by sponging miR-10b-3p to regulate KLF5 expression. *Inflammation* 2020; 43: 1620-33.
29. Jiang H, Toscano JF, Song SS, et al. Differential expression of circulating exosomal microRNAs in refractory intracranial atherosclerosis associated with antiangiogenesis. *Sci Rep* 2019; 9: 19429.
30. Shi Z, Zhang Y, Wang Q, Jiang D. MFG-E8 regulates inflammation and apoptosis in tendon healing, and promotes tendon repair: a histological and biochemical evaluation. *IUBMB Life* 2019; 71: 1986-93.
31. Gao YY, Tao T, Wu D, et al. MFG-E8 attenuates inflammation in subarachnoid hemorrhage by driving microglial M2 polarization. *Exp Neurol* 2021; 336: 113532.
32. Yu L, Zhao L, Jia Z, et al. MFG-E8 overexpression is associated with poor prognosis in breast cancer patients. *Pathol Res Pract* 2019; 215: 490-8.
33. Zhao Q, Xu L, Sun X, et al. MFG-E8 overexpression promotes colorectal cancer progression via AKT/MMPs signalling. *Tumour Biol* 2017; 39: 1010428317707881.
34. Plummer PN, Freeman R, Taft RJ, et al. MicroRNAs regulate tumor angiogenesis modulated by endothelial progenitor cells. *Cancer Res* 2013; 73: 341-52.
35. Du X, Hu N, Yu H, et al. miR-150 regulates endothelial progenitor cell differentiation via Akt and promotes thrombus resolution. *Stem Cell Res Ther* 2020; 11: 354.
36. Liang H, Chen Y, Li H, et al. miR-22-3p suppresses endothelial progenitor cell proliferation and migration via inhibiting onecut 1 (OC1)/vascular endothelial growth factor A (VEGFA) signaling pathway and its clinical significance in venous thrombosis. *Med Sci Monit* 2020; 26: e925482.
37. Uchiyama A, Yamada K, Perera B, et al. Protective effect of MFG-E8 after cutaneous ischemia-reperfusion injury. *J Invest Dermatol* 2015; 135: 1157-65.
38. Wang X, Hao L, Bu HF, et al. Spherical nucleic acid targeting microRNA-99b enhances intestinal MFG-E8 gene expression and restores enterocyte migration in lipopolysaccharide-induced septic mice. *Sci Rep* 2016; 6: 31687.
39. Yang WL, Sharma A, Zhang F, et al. Milk fat globule epidermal growth factor-factor 8-derived peptide attenuates organ injury and improves survival in sepsis. *Crit Care* 2015; 19: 375.
40. Zeng J, Deng Z, Zou Y, et al. Theaflavin alleviates oxidative injury and atherosclerosis progress via activating microRNA-24-mediated Nrf2/HO-1 signal. *Phytother Res* 2021; 35: 3418-27.
41. Lu X, Li H, Wang S. Hydrogen sulfide protects against uremic accelerated atherosclerosis via nPKCdelta/AKT signal pathway. *Front Mol Biosci* 2020; 7: 615816.

42. Cheng Z, Jia W, Tian X, et al. Cotinine inhibits TLR4/NF-kappaB signaling pathway and improves deep vein thrombosis in rats. *Biosci Rep* 2020; 40: BSR20201293.
43. Kotyla PJ, Engelmann M, Giemza-Stoklosa J, Wnuk B, Islam MA. Thromboembolic adverse drug reactions in Janus kinase (JAK) inhibitors: does the inhibitor specificity play a role? *Int J Mol Sci* 2021; 22: 2449.
44. Yu Y, Shen Y, Li J, Liu J, Liu S, Song H. Viral infection related venous thromboembolism: potential mechanism and therapeutic targets. *Ann Palliat Med* 2020; 9: 1257-63.